









RESEARCH ARTICLE

10.1029/2022JA030999

Three-Dimensional Magnetic Reconnection Spreading in Current Sheets of Non-Uniform Thickness

Milton Arencibia¹ , Paul A. Cassak¹ , Michael A. Shay² , Jiong Qiu³ , Steven M. Petrinec⁴ , and Haoming Liang⁵ 

Key Points:

- We derive a theory of three-dimensional spreading of collisionless anti-parallel reconnection in current sheets with non-uniform thickness
- Spreading from a thinner to a thicker current sheet occurs slower than local electron and Alfvén speeds, a key prediction of the theory
- We apply the theory to reconnection spreading in Earth's magnetotail and discuss potential implications for solar flare ribbons

Correspondence to:

M. Arencibia,
milton.arencibia@gmail.com

Citation:

Arencibia, M., Cassak, P. A., Shay, M. A., Qiu, J., Petrinec, S. M., & Liang, H. (2023). Three-dimensional magnetic reconnection spreading in current sheets of non-uniform thickness. *Journal of Geophysical Research: Space Physics*, 128, e2022JA030999. <https://doi.org/10.1029/2022JA030999>Received 11 SEP 2022
Accepted 2 MAR 2023
Corrected 23 MAR 2023

This article was corrected on 23 MAR 2023. See the end of the full text for details.

© 2023. The Authors.

This is an open access article under the terms of the [Creative Commons Attribution-NonCommercial-NoDerivs License](https://creativecommons.org/licenses/by-nc-nd/4.0/), which permits use and distribution in any medium, provided the original work is properly cited, the use is non-commercial and no modifications or adaptations are made.

¹Department of Physics and Astronomy and Center for KINETIC Plasma Physics, West Virginia University, Morgantown, WV, USA, ²Department of Physics and Astronomy, University of Delaware, Newark, DE, USA, ³Department of Physics, Montana State University, Bozeman, MT, USA, ⁴Lockheed Martin Advanced Technology Center, Palo Alto, CA, USA, ⁵Center for Space Plasma and Aeronomic Research (CSPAR), University of Alabama in Huntsville, Huntsville, AL, USA

Abstract Magnetic reconnection in naturally occurring and laboratory settings often begins locally and elongates, or spreads, in the direction perpendicular to the plane of reconnection. Previous work has largely focused on current sheets with a uniform thickness, for which the predicted spreading speed for anti-parallel reconnection is the local speed of the current carriers. We derive a scaling theory of three-dimensional (3D) spreading of collisionless anti-parallel reconnection in a current sheet with its thickness varying in the out-of-plane direction, both for spreading from a thinner to thicker region and a thicker to thinner region. We derive an expression for calculating the time it takes for spreading to occur for a current sheet with a given profile of its thickness. A key result is that when reconnection spreads from a thinner to a thicker region, the spreading speed in the thicker region is slower than both the Alfvén speed and the speed of the local current carriers by a factor of the ratio of thin to thick current sheet thicknesses. This is important because magnetospheric and solar observations have previously measured the spreading speed to be slower than previously predicted, so the present mechanism might explain this feature. We confirm the theory via a parametric study using 3D two-fluid numerical simulations. We use the prediction to calculate the time scale for reconnection spreading in Earth's magnetotail during geomagnetic activity. The results are also potentially important for understanding reconnection spreading in solar flares and the dayside magnetopause of Earth and other planets.

Plain Language Summary Magnetic reconnection is fundamental process in plasmas that converts magnetic energy into kinetic and thermal energy and is known to mediate eruptive solar flares and geomagnetic substorms that create the northern lights. The x-line where magnetic reconnection occurs can elongate or spread over time in the direction normal to the plane of reconnection, and this trait has been observed in the laboratory, Earth's magnetosphere, and is thought to be related to the elongation of chromospheric ribbons during solar flares. This study presents a scaling theory of the three-dimensional (3D) spreading of anti-parallel magnetic reconnection in current sheets with thickness varying in the out-of-plane direction. A key result is that when reconnection spreads from a thinner to a thicker region, the spreading speed in the thicker region is slower than expected. This is important because magnetospheric and solar observations have observed slower spreading speeds than previously predicted, so the present mechanism might explain this feature. We confirm the theory with 3D numerical simulations and use the prediction to calculate the time scale for reconnection spreading in Earth's magnetotail during geomagnetic activity.

1. Introduction

The abrupt release of magnetic energy in substorms in Earth's magnetosphere and flares in the solar corona are key features of the dynamics of these systems and have an important impact on Earth's technological infrastructure. In both processes, magnetic reconnection is the driver of the rapid energy conversion (McPherron et al., 1973; Priest & Forbes, 2000) via a change in magnetic field connectivity (Dungey, 1953; Vasyliunas, 1975). Observations have revealed that reconnecting x-lines (the collection of points where the magnetic field connectivity changes) often start in a localized region of space, and then elongate or spread in time, orthogonal to the reconnection plane in two-ribbon solar flares (Graham & Cauzzi, 2015; Isobe et al., 2002; Qiu, 2009; Qiu et al., 2010, 2017; Tian et al., 2015) and prominence eruptions (Tripathi et al., 2006), at Earth's magnetopause (Walsh et al., 2018; Zhou et al., 2017; Zou et al., 2018), in Earth's magnetotail (Hietala et al., 2014; McPherron et al., 1973; Nagai, 1982;

Nagai et al., 2013), and in laboratory reconnection experiments (Dorfman et al., 2013; Egedal et al., 2011; Katz et al., 2010). Reconnection starting locally and spreading is also thought to happen in the solar wind where x-lines hundreds of Earth radii in extent have been observed (Gosling et al., 2007; Phan et al., 2006; Shepherd et al., 2017).

Most of the previous theoretical and numerical work on the spreading of reconnection has addressed quasi-two-dimensional (2D) anti-parallel reconnection in uniform current sheets with an initial half-thickness w_0 comparable to the ion inertial scale $d_i = c/\omega_{pi}$, where c is the speed of light in vacuum and ω_{pi} is the ion plasma frequency. The consensus is that reconnection spreads orthogonal to the reconnection plane with the velocity of the current carriers (Arencibia et al., 2021; Huba & Rudakov, 2002, 2003; Jain & Büchner, 2017; Jain et al., 2013; Karimabadi et al., 2004; Lapenta et al., 2006; Meyer III, 2013; T. K. M. Nakamura et al., 2012; Shepherd & Cassak, 2012; Shay et al., 2003). This directionality of the spreading is consistent with observations of reconnection during substorms, which spread in the dawnward direction (McPherron et al., 1973; Nagai, 1982; Nagai et al., 2013). While the ions carry most of the current in the quiet plasma sheet, the electrons carry the current when the plasma sheet thins down when reconnection takes place (Jain et al., 2021), so the direction of the spreading is consistent with the direction of the current carriers.

However, reconnecting current sheets in naturally occurring physical systems such as the solar corona and the dayside magnetopause and magnetotail of Earth and other planets are unlikely to have a thickness that is uniform in the out-of-plane direction before reconnection onsets and spreads. For example, in situ observations of the near-Earth magnetotail plasma sheet during quiet times show the half-thickness varies continuously in the dawn-dusk direction from a minimum of $<3 R_E$ at midnight in magnetic local time up to $\sim 8 R_E$ at the flanks, and thins down to $\sim 0.1\text{--}0.4 R_E$ at midnight and $\sim 1 R_E$ at the flanks at the end of a substorm growth phase, before reconnection onset (Fairfield, 1979, 1980; Kaymaz et al., 1994; Sergeev et al., 1990; Tsyganenko, 1998; Voigt, 1984), where R_E denotes the radius of Earth. Thin current sheets where reconnection is more likely to occur are more prevalent on the dusk-side of the magnetotail (Rogers et al., 2023; Rong et al., 2011). Interestingly, however, reconnection is suppressed within $10 d_i$ of the duskward edge of the region undergoing reconnection (Liu et al., 2019), so magnetotail reconnection need not be strongest at the thinnest part of the current sheet. At Earth's dayside magnetopause, the current sheet is thinnest near the nose and gets thicker toward the flanks (Haaland et al., 2014), so reconnection spreads in a non-uniform current sheet. Moreover, in situ observations suggest that magnetosheath high-speed jets can trigger dayside reconnection where the magnetopause current sheet is as thick as $60\text{--}70 d_i$ (Hietala et al., 2018), as corroborated by numerical simulations (Ng et al., 2021), so dayside reconnection also need not begin at the thinnest part of the current sheet. In solar flares, intermittency of the sequential brightening of ribbons has been interpreted as evidence of the nonuniformity in the out-of-plane direction of the flare current sheet (Naus et al., 2022). It has been seen in global magnetospheric simulations that reconnection spreading slows as reconnection spreads from a thinner to a thicker current sheet (Walsh et al., 2018). While there have been numerical studies of a current sheet of non-uniform thickness that was extremely thick outside the reconnection region so that the x-line remained spatially confined (Huang et al., 2020; Liu et al., 2019), we are unaware of any studies that predict the spreading speed of reconnection in current sheets of a non-uniform thickness.

We present a scaling theory of the spreading of collisionless anti-parallel reconnection in current sheets of non-uniform thickness. We include predictions for spreading from a thinner to thicker current sheet and for spreading from a thicker to thinner current sheet. Reconnection may start at its thinnest part, but magnetotail observations suggest that this need not be the case, so both limits are potentially physically relevant. For reconnection that spreads from a thinner into a thicker part of a current sheet, a key result is that the spreading speed in the thicker region is slower than the spreading speed based on current knowledge for a uniform sheet of equivalent local thickness, due to a reduction in the initial effective reconnecting field (Shay et al., 2004). This provides a mechanism for reconnection spreading that is sub-Alfvénic as well as slower than the local current carriers in the macroscopic current sheet. This result is important because observations of dayside reconnection (Zou et al., 2018) and two-ribbon solar flares (Qiu et al., 2017) suggest that the spreading speed is slower than expected from the existing theory. We confirm our prediction with a suite of three-dimensional (3D) two-fluid numerical simulations. We use our prediction for the spreading speed to calculate the time it takes reconnection to spread a particular distance. We apply our results to reconnection in Earth's magnetotail, and motivate potential observational signatures of spreading in current sheets of non-uniform thickness in solar flares.

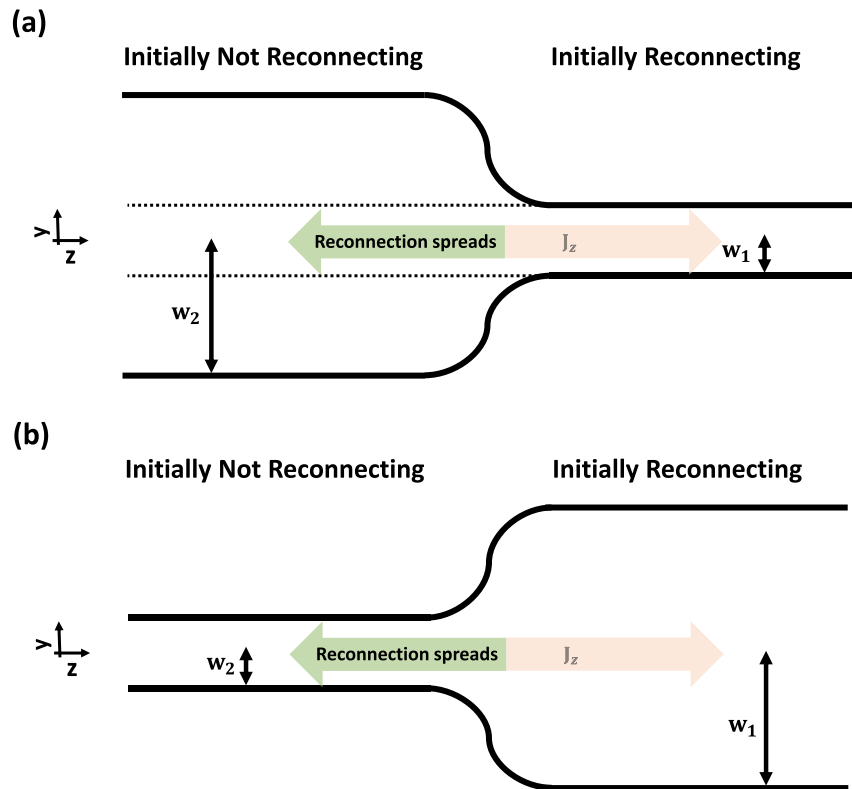


Figure 1. Sketch of the yz plane for a current sheet with non-uniform thickness in the out-of-plane direction in which reconnection spreads from a region of local half-thickness w_1 into a region of half-thickness w_2 , propagated by the electrons carrying the current. Panel (a) is for $w_1 < w_2$ and panel (b) is for $w_1 > w_2$. The dotted lines in panel (a) denote that the reconnected fields that convect into the thicker region essentially remain collimated to a half-thickness w_1 from the thinner region, leading to embedded reconnection because the upstream magnetic field is weaker there.

The layout of this paper is as follows. In Section 2, we present a theory of 3D reconnection spreading in current sheets of non-uniform thickness. In Section 3, we discuss our numerical simulation setup. In Section 4, we discuss the results of our simulations. In Section 5, we apply our results to reconnection in the near-Earth magnetotail and two ribbon solar flares, and offer conclusions in Section 6.

2. Theory

We define a coordinate system in which z is the out-of-plane direction coincident with the direction of the initial current density J_z , x is the direction of the equilibrium reversing magnetic field, and y completes a right-handed coordinate system. We use a reference frame where the electrons fully carry the initial current for simplicity and treat collisionless reconnection. We assume the reconnecting magnetic field B_x asymptotes to a magnitude of B_0 at all values of z for simplicity.

The current sheet has a half-thickness $w(z)$ in the y -direction that varies in the out-of-plane direction. Representative sketches of the current sheet profile in the yz plane are shown in Figure 1. The solid black lines represent the edge of the equilibrium current layer, and the green arrow denotes the direction that reconnection spreads due to the electron current carriers. Panel (a) depicts a current sheet with a monotonically increasing current sheet half-thickness, for which reconnection spreads from a thinner to thicker region of the current sheet, while panel (b) depicts a current sheet with a monotonically decreasing current sheet half-thickness, for which spreading is from a thicker to thinner region. We define the current sheet half-thickness where reconnection starts as w_1 . In the simulations we use to test the theory, the current sheet half-thickness asymptotes to w_2 . We assume the half-thickness $w(z)$ varies slowly as a function of z , and we will quantify this condition in what follows. We first introduce general aspects of the derivation of the spreading speed. Then, we separately calculate the spreading speed as a function of $w(z)$ for monotonically increasing and decreasing thickness profiles.

2.1. General Considerations of Reconnection Spreading in Current Sheets of Non-Uniform Thickness

We begin with a review of the analysis of the spreading speed for anti-parallel reconnection in a current sheet of uniform thickness in Arencibia et al. (2021). Spreading occurs because the reconnected (y) component of the magnetic field propagates in the direction of the current carriers, triggering the sequential onset of reconnection and causing the x -line to grow in length. This is governed by Faraday's law, given in cgs units as

$$\frac{\partial B_y}{\partial t} \simeq -c \frac{\partial E_x}{\partial z}, \quad (1)$$

where \mathbf{B} is the magnetic field, \mathbf{E} is the electric field, and the variation of E_x in the x -direction is assumed to be small. In a small interval of time Δt , B_y propagates a distance Δz in the z direction, and the spreading speed is defined as $v_s = \Delta z / \Delta t$. It is estimated from a scaling analysis of Equation 1, giving

$$v_s \sim -c \frac{\Delta E_x}{\Delta B_y}. \quad (2)$$

For anti-parallel reconnection, it was argued that the main contributor to E_x is the Hall electric field $-J_z B_y / nec$ (Arencibia et al., 2021), where n is the upstream density and e is the elementary charge, so that

$$v_s \sim c \frac{\Delta(J_z B_y / nec)}{\Delta B_y}. \quad (3)$$

For a current sheet of uniform thickness, J_z and n are independent of z , so Equation 3 becomes

$$v_s \sim \frac{J_z}{ne}. \quad (4)$$

This result provided a first-principles scaling prediction of the previously known result that spreading of anti-parallel reconnection in a current sheet of uniform thickness occurs at the speed of the current carriers (Huba & Rudakov, 2002, 2003; Jain et al., 2013; Shay et al., 2003). Since $J_z \sim c B_0 / 4\pi w$, Equation 4 gives

$$v_s \sim \frac{c B_0}{4\pi n e w} \sim \frac{c_{A0} d_i}{w}, \quad (5)$$

where $d_i = c / \omega_{pi} = (m_i c^2 / 4\pi n e^2)^{1/2}$ is the ion inertial scale, $c_{A0} = B_0 / (4\pi n m_i)^{1/2}$ is the Alfvén speed based on B_0 , and m_i is the ion mass.

We now show how to generalize this theory for spreading in a current sheet of non-uniform thickness, where v_s is expected to be a function of z . Equations 1–3 are unchanged, but when $w(z)$ is non-uniform, $J_z(z)$ is no longer uniform. Continuing to treat n as uniform for simplicity, using the chain rule in Equation 3 gives

$$v_s(z) \sim \frac{1}{ne} \left[J_z(z) + B_y(z) \frac{\Delta J_z(z)}{\Delta B_y(z)} \right], \quad (6)$$

where we have made the z dependence explicit. Since $B_y \simeq 0$ in the non-reconnecting region, B_y is on the same order of magnitude as ΔB_y , so the second term in the brackets scales like ΔJ_z while the first scales like J_z . If $w(z)$ varies rapidly, the second term would need to be retained and may even dominate. However, since we are assuming that $w(z)$ varies slowly, we argue that $\Delta J_z \ll J_z$, and the second term can be neglected. In this limit, the spreading speed is

$$v_s(z) \sim \frac{J_z(z)}{ne} \simeq \frac{c_A(z) d_i}{w(z)}. \quad (7)$$

where we use Ampère's law to write $J_z(z) \simeq c B_x(z) / 4\pi w(z)$ and define the Alfvén speed as a function of z as $c_A(z) = B_x(z) / (4\pi n m_i)^{1/2}$, where the reconnecting magnetic field B_x can depend on z . We argue in what follows that $B_x(z)$ depends on whether the current sheet half-thickness is increasing or decreasing.

2.2. Spreading From a Thinner to a Thicker Current Sheet

We first consider the system sketched in Figure 1a, with reconnection beginning in a region of uniform half-thickness w_1 that spreads monotonically into a thicker region. We argue that the reconnected magnetic field

B_y is collimated at a half thickness near w_1 as it spreads into the thicker current sheet. Reconnection initiates in a plane of given z when B_y appears at that z . In the next increment in time Δt , B_y convects a small distance Δz . Since the equilibrium current sheet thickness increases with z , the half-thickness expands from $w(z)$ to $w(z + \Delta z)$. The perturbing B_y is expected to also broaden as it goes from z to $z + \Delta z$. If the vertical inflow speed v_y due to reconnection exceeds the speed of the broadening of B_y due to the increase of the half-thickness of the current sheet, then B_y remains collimated as it convects to $z + \Delta z$. Data supporting this statement will be given in Section 4.

We now develop a quantitative condition for B_y to remain collimated. Between the thin and thick parts of the current sheet, the reconnecting magnetic field B_x has a gradient in the z direction that is associated with a vertical equilibrium current $J_{y,eq} = (c/4\pi)\partial B_x/\partial z$. The associated vertical velocity $v_{ey,eq}$ due to the equilibrium flow which serves to broaden B_y scales as

$$v_{ey,eq} \sim -\frac{J_{y,eq}}{ne} \sim -\frac{c}{4\pi ne} \frac{\partial B_x}{\partial z}. \quad (8)$$

We estimate this speed at $y = w(z)$. Suppose the B_x profile is written as $B_x(y, z) = B_0 \tilde{B}_x[y/w(z)]$, where \tilde{B}_x is a dimensionless function capturing the spatial structure of B_x . Using the chain rule, $\partial B_x/\partial z = B_0 \tilde{B}'_x[\partial(y/w)/\partial w](dw/dz)$, where \tilde{B}'_x is the derivative of \tilde{B}_x with respect to its argument. Evaluating this at $y = w$ gives $\partial(y/w)/\partial w = -1/w$, so we get $\partial B_x[y = w(z), z]/\partial z = -B_0 \tilde{B}'_x(1)(1/w)(dw/dz) = -B_0 \tilde{B}'_x(1)/w_z$, where $w_z = [d \ln(w)/dz]^{-1}$ is the scale size over which the half-thickness of the current sheet changes. Then, the scaling of Equation 8 gives

$$v_{ey,eq} \sim \frac{c_{A0} d_i \tilde{B}'_x(1)}{w_z}. \quad (9)$$

Letting the inflow speed associated with the reconnection be v_{in} , we find that B_y remains collimated if $v_{in} > v_{ey,eq}$, that is,

$$w_z > \frac{c_{A0}}{v_{in}} \tilde{B}'_x(1) d_i. \quad (10)$$

v_{in}/c_{A0} is a proxy for the reconnection rate, which we expect to be on the order of 0.1. Since $\tilde{B}'_x(1)$ is typically of order 1, we find that the condition that B_y remains collimated as it enters a thicker current sheet is w_z is at least around $10 d_i$. For most physical systems of interest, this is a small scale compared to the size of upstream structures, so it is likely this condition is satisfied. If such small-scale structure did occur, it would be prone to kinetic instabilities that smooth out sharp gradients. Consequently, we expect B_y to remain collimated at the thinner scale w_1 as it spreads into regions with a thicker current sheet. This collimation is sketched as the dotted lines in Figure 1a.

This result implies the magnetic field outside the region of half-thickness $y > w_1$ is not significantly perturbed by B_y and does not initially participate in the reconnection in the thicker region, provided the time scale for spreading is shorter than the time scale for the current sheet to collapse due to reconnection. Consequently, the effective upstream magnetic field that controls the driving of the reconnection process is weaker than the asymptotic magnetic field B_0 . Reconnection for which only a thinner sublayer participates in the reconnection process has previously been referred to as “embedded” (Cassak & Drake, 2009; Shay et al., 2004).

We can estimate the spreading speed semi-empirically. We hypothesize that the effect of embedding is that $B_x(z)$ is lower than B_0 in Equation 7 for the spreading speed. We estimate the reconnecting magnetic field $B_x(z)$ that initially participates in reconnection by assuming B_x varies approximately linearly in y within the current layer (Shay et al., 2004), so that the reconnecting magnetic field in a current sheet of thickness $w(z)$ is

$$B_x(z) \sim B_0 \frac{w_1}{w(z)}. \quad (11)$$

The subsequent spreading speed from Equation (7) using $c_A(z) = B_x(z)/(4\pi m_i n)^{1/2}$ is

$$v_s(z) = \frac{c_{A0} d_i w_1}{[w(z)]^2}. \quad (12)$$

Therefore, the predicted spreading speed $v_s(z)$ at a position z is slower than the spreading speed for a current sheet of equivalent uniform half-thickness $w(z)$, given by $c_A d_i/w(z)$, by a factor of $w_1/w(z)$. This is a key prediction of this theory and a departure from previous knowledge of reconnection spreading in current sheets of uniform

thickness. It shows the spreading speed fundamentally depends not just on the local current sheet half-thickness $w(z)$, but there is also a “memory” effect of the current sheet from where its half-thickness was w_1 .

2.3. Spreading From a Thicker to a Thinner Current Sheet

If reconnection spreads from a thick region into a thinner one as sketched in Figure 1b, the incoming reconnected magnetic field B_y perturbs the entire thickness of the thinner region. The full thickness of the thinner current layer participates in reconnection from the beginning, and thus the relevant upstream magnetic field is the asymptotic magnetic field B_0 . This implies that $c_A(z) = c_{A0}$, a constant, in Equation 7, so the spreading speed prediction is

$$v_s(z) \simeq \frac{c_{A0} d_i}{w(z)}. \quad (13)$$

This implies that reconnection in this scenario spreads in the thinner region at a speed given by the local current carrier speed. Thus, in contrast to spreading from a thinner to thicker current sheet, spreading from a thicker to thinner current sheet has no memory effect.

2.4. Time Scale for Spreading a Prescribed Distance

Since the speed is a function of position for spreading in non-uniform current sheets, it is challenging to test the spreading speed prediction numerically, experimentally, or observationally by direct measurement. Thus, we also provide a prediction for the time it takes for spreading to occur over some region, which is likely to be easier to measure. From elementary mechanics, the time τ it takes to spread from position z_1 to z_2 is

$$\tau = \int_{z_1}^{z_2} \frac{dz}{v_s(z)}, \quad (14)$$

where the appropriate form of $v_s(z)$ needs to be used for thinner-to-thicker or thicker-to-thinner current sheet thickness profiles.

While Equation 14 is expected to be valid for any gradually changing thickness profile $w(z)$, we exemplify the procedure by assuming a half-thickness profile $w(z)$ of the power law form

$$w(z) = w_1 + (w_2 - w_1) \left(\frac{z}{\Delta z} \right)^\alpha, \quad (15)$$

where $\Delta z = z_2 - z_1$, $z_1 = 0$, and α is a dimensionless parameter that can be chosen for a particular model current sheet. Here, $w(z_1) = w_1$ and $w(z_2) = w_2$. We first consider spreading from a thinner to thicker current sheet. Using Equation 15 in Equation 12, the integral in Equation 14 straight-forwardly gives

$$\tau = \frac{w_1 \Delta z}{c_A d_i} \left[1 + 2 \frac{w_2/w_1 - 1}{\alpha + 1} + \frac{(w_2/w_1 - 1)^2}{2\alpha + 1} \right]. \quad (16)$$

To interpret this result, we note that the prefactor is the transit time for reconnection spreading in a uniform current sheet of half-thickness w_1 over a distance Δz . Therefore, the α -dependent and w_2 -dependent terms in the brackets represent a geometric factor that describes the increase in the spreading time due to the current sheet becoming thicker.

Similarly, for reconnection spreading in a current sheet that decreases in half-thickness gradually from w_1 to w_2 with a profile according to Equation 15, the local spreading speed is instead given by Equation 13. Then, the integral in Equation 14, after simplifying, gives

$$\tau = \frac{w_1 \Delta z}{c_A d_i} \left(1 + \frac{w_2/w_1 - 1}{\alpha + 1} \right). \quad (17)$$

3. Simulation Setup

The simulation study is carried out using the two-fluid code F3D (Shay et al., 2004), which updates the continuity, momentum, induction, and pressure equations, and includes the Hall and electron inertia terms in the generalized

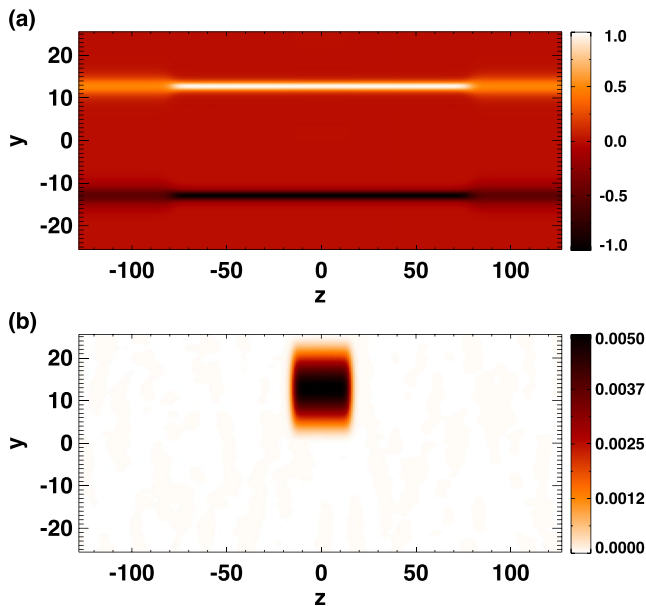


Figure 2. Representative initial conditions for a simulation with a current sheet with thickness that varies in the out-of-plane direction. The plots give a cut in the yz plane at $x = -L_x/2$ of (a) the initial current density J_z with a thickness profile given by Equation 18 with $w_1 = 1$ and $w_2 = 2$, and (b) the y -component of the magnetic perturbation B_{1y} .

Ohm's law to account for separate electron and ion dynamics below the ion inertial scale. Time is stepped forward using the trapezoidal leapfrog algorithm (Guzdar et al., 1993) and spatial derivatives are fourth-order finite differences. Lengths are normalized to the ion inertial scale $d_{i0} = (m_i c^2 / 4\pi n_0 e^2)^{1/2}$, time is normalized to the inverse ion cyclotron frequency $\Omega_{ci0}^{-1} = m_i c / e B_0$, velocities to the Alfvén speed $c_{A0} = B_0 / \sqrt{4\pi m_i n_0}$, electric fields to $c_{A0} B_0 / c$, current densities to $c B_0 / 4\pi d_{i0}$, and temperatures to $m_i c_{A0}^2 / k_B$, where B_0 is the initial asymptotic strength of the reversing magnetic field, n_0 is the initial upstream density, and k_B is Boltzmann's constant.

For this study, we employ an identical simulation setup as our anti-parallel reconnection simulations in an earlier study (Arencibia et al., 2021) with the exception of a non-uniform current sheet thickness profile. We use a computational domain with dimensions $L_x \times L_y \times L_z = 102.4 \times 51.2 \times 256.0$ with triply periodic boundary conditions. The grid scale is $\Delta x \times \Delta y \times \Delta z = 0.05 \times 0.05 \times 1.0$. The time step is 0.02 and the ion-to-electron mass ratio is $m_i / m_e = 25$ for all simulations in this study.

For our initial conditions, we employ two oppositely directed current sheets with the x -component of the initial magnetic field given by $B_{0x} = \tanh[(y + L_y/4)/w_0(z)] - \tanh[(y - L_y/4)/w_0(z)] - 1$, so that the two current sheets are centered at $y = \pm y_{cs} = \pm L_y/4$, which permits the use of periodic boundary conditions. Here, $w_0(z)$ is the initial current sheet half-thickness profile, which varies in the out-of-plane direction between two specified values w_1 and w_2 , given by

$$w_0(z) = \frac{w_1 + w_2}{2} + \frac{w_1 - w_2}{2} \left[\tanh\left(\frac{z + L_0}{w_z}\right) - \tanh\left(\frac{z - L_0}{w_z}\right) - 1 \right], \quad (18)$$

where $z = 0$ is the center of the computational domain, $L_0 = 80$ is the half-length in the out-of-plane direction of the region of half-thickness w_1 , and $w_z = 4$ (unless otherwise stated) is the gradient scale length over which the half-thickness changes from w_1 to w_2 . The full extent of the region over which the current sheet changes from a half-thickness of w_1 to w_2 is $\Delta z = 2w_z$, which for all simulations in this study is large enough to satisfy Equation 10. We carry out two suites of simulations, one holding $w_1 = 1.0$ fixed and varying $w_2 = 1.25, 1.5, 1.75, 2$ (all thinner to thicker), and another holding $w_2 = 2$ fixed and varying $w_1 = 0.75, 1.5, 1.75, 1.9, 2.25, 2.5$ (a combination of thinner to thicker and thicker to thinner). We also carry out one simulation with $w_1 = 2.0$ and $w_2 = 1.5$ (thicker to thinner) and an additional two simulations with uniform half-thicknesses $w_0 = 1.0$ and 2.0 . Thicker initial current sheets are desirable but, because they take longer to evolve, are significantly more computationally expensive. Figure 2a shows initial conditions for the out-of-plane current J_z in a cut in the yz plane at $x = -L_x/2$, showing distinct regions of different half-thicknesses $w_1 = 1$ and $w_2 = 2$, analogous to the sketch in Figure 1. The initial density is uniform, and the initial profile of the temperature is non-uniform, varying from 1 to 1.5, with a profile chosen to balance total pressure (plasma plus magnetic) to ensure the profile is in MHD equilibrium. The fluid pressure is provided fully by ions and is treated as adiabatic, while electrons are assumed cold at all times and carry all of the initial current.

We initialize all simulations with a coherent perturbation in the magnetic field, for which the z component of the magnetic vector potential A_{1z} is

$$A_{1z}(x, y, z) = \frac{\tilde{B}_1}{4\pi L_y} \left[1 + \cos\left(\frac{4\pi(y - L_y/4)}{L_y}\right) \right] \sin\left(\frac{2\pi x}{L_x}\right) f(z) \quad (19)$$

for $y \geq 0$ and 0 for $y < 0$, where $\tilde{B}_1 = 0.005$ is a constant and the envelope $f(z)$ has the form

$$f(z) = \frac{1}{2} \left[\tanh\left(\frac{z + w_{0pert}}{2}\right) - \tanh\left(\frac{z - w_{0pert}}{2}\right) \right], \quad (20)$$

where $w_{0pert} = 15$ is the initial half-length of the coherent perturbation in the out-of-plane direction. The resulting magnetic perturbation $\mathbf{B}_1 = -\hat{\mathbf{z}} \times \nabla A_{1z}$ creates an x-line/o-line pair in the xy plane for only the upper current sheet at $y = y_{cs} = L_y/4$, localized to $-w_{0pert} < z < w_{0pert}$. Figure 2b shows a cut in the yz plane at $x = -L_x/2$ of the

y -component of the coherent perturbation in the magnetic field. The value of w_{pert} is chosen to ensure the perturbation is localized exclusively in the region of half-thickness w_1 so that any reconnection observed in the region of half-thickness w_2 is due to spreading of reconnection and not due to the initial perturbation. We perturb only the upper current sheet to prolong the timescale for the interaction between the two current sheets resulting from flows in the y -direction and thus ensure the reconnection occurring in the upper sheet at later times is not caused by the lower current sheet.

Incoherent noise in the x and y components of the magnetic field at the 10^{-5} level is included to break symmetry, which prevents secondary magnetic islands from staying at the initial x -line location (e.g., Shay et al., 2004). A fourth-order diffusion term is included in all equations with coefficients $D_{4x} = D_{4y} = 1.6 \times 10^{-5} d_{i0}^4 \Omega_{ci0}^{-1}$ in the x -direction and y -direction and a larger diffusion coefficient in the z -direction $D_{4z} = 1.6 \times 10^{-1}$ due to the larger grid scale. These values are varied in trial simulations to ensure they do not play any significant role in the numerics.

4. Results

We begin by testing the spreading speed prediction in Equations 12 and 13. First, we discuss how we find where reconnection is taking place in our 3D simulations and how we determine the speed at which the reconnection spreads.

The strength of the normal magnetic field component B_y near the reconnection region is an indicator of the presence of reconnection (Arencibia et al., 2021; Huba & Rudakov, 2002; Jain & Büchner, 2017; Li et al., 2020). The average magnitude of B_y at the left and right downstream edges of the electron diffusion region is a proxy for the reconnection rate; we denote this quantity as $\tilde{B}_y(z, t)$, given by

$$\tilde{B}_y(z, t) = \frac{|B_y(\tilde{x} + L, y_{cs}, z, t)| + |B_y(\tilde{x} - L, y_{cs}, z, t)|}{2}, \quad (21)$$

where \tilde{x} is the x location of the x -line in the plane specified by z at time t and $L \sim 2$ is the approximate half-length of the electron diffusion region. For further details, see sec. IV D in Arcencibia et al. (2021).

The average reconnected field $\tilde{B}_y(z, t)$ for the upper current sheet ($y = y_{cs} = L_y/4$) is shown in Figure 3 as a stack plot as a function of time t and out-of-plane coordinate z over the whole domain for four 3D simulations with non-uniform thickness. Panels (a) through (d) have $w_2 = 1.25, 1.5, 1.75,$ and 2.0 in the thicker part of the current sheet, respectively, and all four have $w_1 = 1$ in the thinner part. Each horizontal cut represents data from a fixed xy plane as a function of time t , while each vertical cut represents the spatial extent of \tilde{B}_y in the z direction of the reconnecting region at a fixed time. The triangular shape of $\tilde{B}_y(z, t)$ seen in Figure 3 is a characteristic of reconnection that is spreading uni-directionally (Shay et al., 2003; Shepherd & Cassak, 2012), as the extent of the reconnection region increases in time. We see \tilde{B}_y increase in time from 0 to an asymptotic value of ≈ 0.1 when reconnection reaches a quasi-steady state in the current sheet region with local half-thickness w_1 before spreading in the $-z$ -direction into the region with local half-thickness w_2 .

We define the onset of fast reconnection at a given xy plane to be when \tilde{B}_y exceeds 0.04, after which reconnection proceeds to a quasi-steady state (Arencibia et al., 2021). Onset times for individual xy planes are plotted in Figure 3 as black triangles for a chosen range of z values in the region of initial half-thickness w_2 . The spreading speeds v_{s2} in the region of uniform half-thickness w_2 are simply the slope of the collection of points denoting the onset time. We determine this slope using a least squares fit and the slopes are shown as the white lines in each panel of Figure 3. The spreading speed v_{s1} in the region of half-thickness $w_1 = 1$ for all four simulations in Figure 3 is ≈ 1.0 (not shown), which is consistent with Equation 5 as expected (Huba & Rudakov, 2002; Shay et al., 2003). In all four cases, there is a break in the spreading speed where the reconnection reaches the region of larger half-thickness w_2 and all show spreading speeds well below $c_{A0} d_{i0} / w_2$, which would be the expected spreading speed if the uniform current sheet spreading speed theory (Huba & Rudakov, 2002; Shay et al., 2003) was valid for current sheets of non-uniform thickness.

Stack plots analogous to those in Figure 3 are generated and spreading speeds are obtained using the same method for all the simulations in this study (not shown). Table 1 gathers the results for all simulations in this study in the first column, labeled as ordered pairs (w_1, w_2) according to their respective current sheet half-thicknesses. We

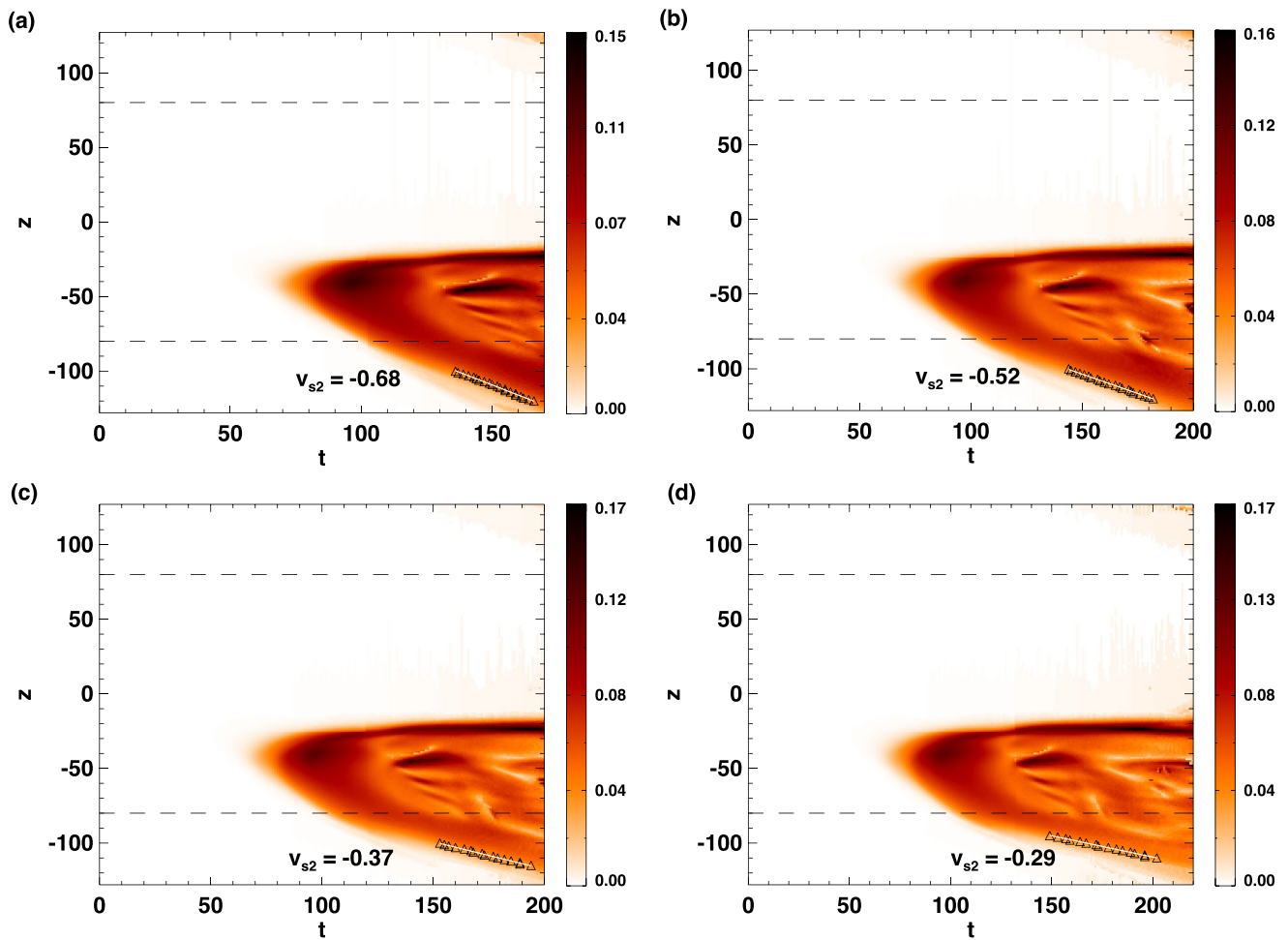


Figure 3. Average reconnected magnetic field $\bar{B}_y(z, t)$, defined in Equation 21, as a function of the out-of-plane direction z and time t , for simulations with initial non-uniform current sheet half-thicknesses $w_1 = 1$ for $-80 < z < 80$ and opening out to $w_2 =$ (a) 1.25, (b) 1.5 (c) 1.75, and (d) 2 elsewhere, where distances are in units of d_{i0} and times are in Ω_{ci0}^{-1} . The dashed lines separate the regions of different thicknesses, where w_1 is localized within $-80 < z < 80$ and w_2 elsewhere. Spreading in the thinner region of current sheet thickness w_1 occurs between $t = 80$ and 100. The spreading is slower in the region of thickness w_2 . Black triangles denote when and where $\bar{B}_y = 0.04$ for a chosen range in z in the region of initial half-thickness w_2 . The out-of-plane reconnection spreading speed v_{s2} in the region with half-thickness w_2 , listed for each simulation in units of c_{A0} , is the best fit slope of these points, shown as a white line.

include the spreading speed prediction from Equations 12 and 13 in the region of half-thickness w_2 in the second column for simulations with $w_1 < w_2$ and $w_1 > w_2$, respectively. The third column is the calculated spreading speed magnitude v_{s2} from the simulations and the fourth column is the deviation from the theoretical prediction shown as a percentage.

We gather the spreading speeds from our simulations in Figure 4. Panel (a) shows v_{s2} as a function of the current sheet half-thickness w , which represents either independent variables w_1 or w_2 , depending on which is the independent variable for the given set of simulations. The two uniform half-thickness simulations $(w_1, w_2) = (1, 1)$ and $(2, 2)$ are shown as blue crosses. The three simulations with $w_1 = 1$ and $w_2 = 1.25, 1.5,$ and 1.75 are shown as black squares and the independent variable is $w = w_2$. The five simulations with $w_1 = 0.75, 1.0, 1.25, 1.5,$ and 1.9 and $w_2 = 2$ are shown as red triangles and the two simulations with $w_1 = 2.25, 2.5$ and $w_2 = 2$ are shown as red asterisks, where the independent variable is $w = w_1$. The dashed black line represents the theoretical prediction from Equation 12 for simulations with $w_1 = 1$ fixed with $w = w_2$ as the independent variable. The red dash-dot piecewise-curve represents the prediction from Equation 12 with $w_2 = 2$ fixed with $w = w_1$ as the independent variable for $w_1 < w_2$, and Equation 13 for $w_1 > w_2$. The simulation results are in excellent agreement with the theory. The $(w_1, w_2) = (2, 1.5)$ simulation is not expected to lie on either of the two curves and thus is not shown.

Table 1
Results for 3D Two-Fluid Simulations in This Study

(w_1, w_2)	Predicted v_{s2}	Measured v_{s2}	Deviation (%)
(1.0, 1.0)	1.00	0.97	-3.1
(2.0, 2.0)	0.50	0.51	2.0
(1.9, 2.0)	0.48	0.41	-15.9
(1.75, 2.0)	0.44	0.38	-15.1
(1.5, 2.0)	0.38	0.31	-21.0
(1.0, 2.0)	0.25	0.29	13.8
(0.75, 2.0)	0.19	0.26	-27.9
(1.0, 1.25)	0.64	0.68	5.9
(1.0, 1.5)	0.44	0.52	14.5
(1.0, 1.75)	0.33	0.37	11.7
(2.25, 2.0)	0.50	0.46	-8.0
(2.5, 2.0)	0.50	0.51	2.0
(2.0, 1.5)	0.67	0.73	9.5

Note. The first column gives ordered pairs (w_1, w_2) for current sheets that vary in half-thickness along the out-of-plane direction from a value of w_1 to w_2 in units of d_{i0} . v_{s2} is the reconnection spreading speed in the region with half-thickness w_2 . The second column gives the theoretical predictions from Section 2, and the third column gives the values measured from the simulations. The deviation from the theory is shown as a percentage in the fourth column.

To test the agreement more quantitatively, Figure 4b shows spreading speeds v_{s2} for all simulations with $w_1 \leq w_2$ as a function of w_1/w_2^2 , the predicted dependence from Equation 12. We calculate a linear least squares fit of these points and show the fit as a dashed line with a functional form $v_{s2} = (0.919 \pm 0.082)w_1/w_2^2 + (0.044 \pm 0.041)$, showing excellent agreement with Equation 12. Simulations with $w_1 > w_2$ are not included in the fit as they are predicted to satisfy a different scaling. We conclude the theory of spreading speeds in a current sheet varying in thickness from w_1 to w_2 are consistent with the predictions in Section 2.

We use the same simulations to test our prediction for spreading in current sheets with a thickness that varies continuously in the out-of-plane direction. To compare with Equation 16, we estimate the spreading timescale in the region where the current sheet thickness changes in the simulation with $(w_1, w_2) = (1, 2)$. The stack plot for the simulation in Figure 3d shows that reconnection spreads across the region $-84 < z < -76$ approximately over the time range $100 < t < 120$, so $\tau \approx 20$. From Equation 18, the thickness varies approximately linearly across the transition region $-84 < z < -76$, so we use $\alpha = 1$ and $\Delta z = 2w_z = 8$. Using Equation 16, the spreading time across the region where the current sheet thickness changes is predicted to be $\tau \approx 19$. This is in good agreement with the simulation results. To further test the theory, two additional simulations with $(w_1, w_2) = (1, 2)$ are performed using $w_z = 8$ and $w_z = 12$ for the gradient length scale in Equation 18, doubling and tripling Δz . The spreading timescales in the higher w_z simulations increase approximately by factors of 2 and 3, respectively (not shown). This is in agreement with the predicted scaling with Δz in Equation 16 assuming the same linear profile with $\alpha = 1$. These results suggest that the theory for the spreading speed in current sheets with a gradually varying thickness is valid.

Finally, we confirm the assumption that the reconnected magnetic field B_y is collimated for spreading from a thinner to a thicker current sheet. We do this by a visual inspection of B_y in the thick part of a non-uniform current sheet and compare it with a simulation with a uniform and equal local thickness. Figure 5 shows cuts of B_y in the yz plane at $x = \bar{x} - L$ where $L = 2$ is the approximate half-length of the electron diffusion region, taken at representative times when B_y approximately reaches the $z = -115$ plane with an amplitude comparable to the initial perturbation ~ 0.004 for (a) a simulation with uniform thickness $w_0 = 2$ at $t = 280$ and (b) the simulation with $w_1 = 1$ and $w_2 = 2$ at $t = 170$. The color bar is saturated at a relatively weak value of $B_y = 0.01$ to resolve the very weak magnetic fields spreading in the out-of-plane direction (right to left). Focusing on the saturated (white) colors, panel (b) shows that B_y is significantly collimated in the y direction around the current sheet center $y = 12.8$ when compared to the uniform case in panel (a), hence initially perturbing only a smaller embedded portion of the magnetic field, illustrating the assumption of the theory. A similar comparison was carried out between the simulation with uniform thickness $w_0 = 2$ at $t = 280$ and the simulation with $w_1 = 1.5$ and $w_2 = 2$ at $t = 255$ (not shown). For this comparison with more similar thicknesses w_1 and w_2 , no appreciable difference in the thickness of the convected B_y could be seen in the two simulations. We attribute this to the spatial scale of the collimation being too similar for differences to be resolved. Uncertainties in the time slices used for the comparison also make it challenging to discern the collimation of B_y for this comparison. In summary, a simulation with sufficient scale separation shows clear evidence that the reconnected B_y is collimated as it convects.

5. Applications

5.1. Reconnection Spreading in the Near-Earth Magnetotail

The central plasma sheet in the near-Earth magnetotail is known to vary in thickness continuously in the dawn-dusk direction Y_{GSM} in the Geocentric Solar Magnetospheric (GSM) coordinate system, equivalent to the z coordinate in Section 2. It has a minimum thickness at midnight magnetic local time and maxima at the flanks near the nightside magnetopause (see fig. 3 in Voigt (1984) and fig. 7 in Tsyganenko (1998)). Thin current sheets are more commonly found from midnight to dusk (Rogers et al., 2023). The anti-parallel field configuration and low collisionality make it an ideal system to apply the theory.

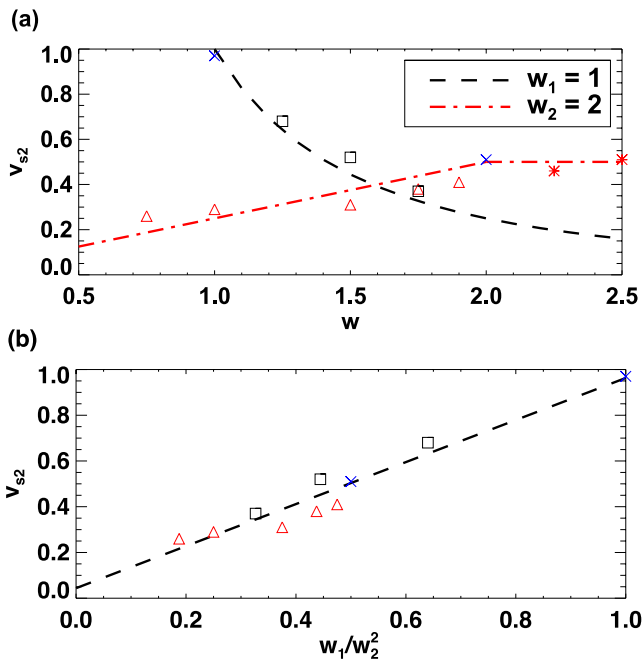


Figure 4. Comparison of simulation results and theory for the reconnection spreading speed v_{s2} in units of c_{A0} in the region where the initial current sheet half-thickness is w_2 in units of d_{i0} for anti-parallel reconnection simulations with current sheets that vary in the out-of-plane direction from a half-thickness w_1 to w_2 . (a) v_{s2} as a function of the current sheet half-thickness w , which represents either independent variables w_1 or w_2 , depending on which is the independent variable for the given set of simulations. Two uniform half-thickness simulations $(w_1, w_2) = (1, 1)$ and $(2, 2)$ are shown as blue crosses. Three simulations with $w_1 = 1$ and $w_2 = 1.25, 1.5,$ and 1.75 are shown as black squares and the independent variable is $w = w_2$. Five simulations with $w_1 = 0.75, 1.0, 1.25, 1.5, 1.75, 1.9,$ and $w_2 = 2$ are shown as red triangles and two simulations with $w_1 = 2.25, 2.5$ and $w_2 = 2$ are shown as red asterisks, where the independent variable is $w = w_1$. The dashed black line represents the theoretical prediction from Equation 12 for simulations with $w_1 = 1$ fixed with $w = w_2$ as the independent variable. The red dash-dot piecewise-curve represents the prediction from Equation 12 with $w_2 = 2$ fixed with $w = w_1$ as the independent variable for $w_1 < w_2$, and Equation 13 for $w_1 > w_2$. (b) v_{s2} as a function of w_1/w_2^2 for simulations with $w_1 \leq w_2$. The dashed black line gives the theoretical prediction from Equation 12.

First, we compute the timescale for magnetic reconnection to spread during a substorm expansion event in the near-Earth magnetotail. For pre-substorm initial conditions, assuming a fully ionized hydrogen plasma, a reconnecting magnetic field with an asymptotic value $B_x \approx 20$ nT (Miyashita et al., 2020) and a magnetosphere density at the plasma sheet boundary layer of $n \approx 0.1$ cm $^{-3}$ (Baumjohann et al., 1990), we estimate the ion inertial scale is $d_i \approx 720$ km and the Alfvén speed is $c_A \approx 1,400$ km s $^{-1}$. We take $w_1 \approx 0.1 - 0.4R_E \approx 0.89 - 3.5 d_i$ as the minimum cross-tail half-thickness at midnight and $w_2 \approx 1R_E \approx 8.9 d_i$ as the maxima at the flanks, and $\Delta z \sim 15R_E \approx 133d_i$ as the approximate half-length of the cross-tail current sheet along the dawn-dusk direction (Fairfield, 1980; Sergeev et al., 1990). Since Δz greatly exceeds the ion inertial scale, the assumption that the current sheet only gradually becomes thicker is valid. We assume reconnection begins with a finite x-line with its downward edge situated at midnight ($Y_{GSM} = 0$), such that reconnection spreads downwards in the direction of electron motion (Nagai et al., 2011, 2013) until reaching $Y_{GSM} = -\Delta z = -15R_E$. Assuming a parabolic cross-tail current sheet, we use $\alpha = 2$ in Equation 15. Using Equation 16, this gives spreading timescales in the range $\tau \approx 2.5 - 23.6$ min, where the range depends on the value for w_1 . For comparison, if the cross-tail current sheet were uniform with a typical midnight half-thickness $w_1 \approx 0.1 - 0.4 R_E \approx 0.89 - 3.5 d_i$, Equation 5 implies the timescale for spreading would be in the range of $\tau \approx 1 - 4$ min, comparable to the Alfvén crossing time ≈ 1 min. Thus the theory provides a mechanism for reconnection spreading along the cross-tail current sheet on timescales longer than both what Alfvén and current carrier speeds suggest.

Observations also suggest that reconnection in the near-Earth magnetotail may begin with an x-line with its downward edge at $Y_{GSM} > 0$ (Nagai et al., 2013; R. Nakamura et al., 2004; Shay et al., 2003). This suggests reconnection may first spread from a thicker part of the current sheet into the thinner part at midnight before continuing to spread downwards toward a thicker part of the current sheet. In this scenario, the timescale for spreading in the $Y_{GSM} > 0$ region would be calculated with Equation 17 for spreading along the region of decreasing current sheet thickness.

There is also observational evidence that reconnection may not spread across the entire dawn-dusk direction, instead stopping when the x-line is $\sim 8R_E$ in length (Nagai et al., 2013). Constraining Δz to empirical values in Equations 16 and 17 may give more accurate predictions. We point out that the structure of the cross-tail current sheet may also be more complex and bend away from the dawn-dusk direction asymmetrically near the flanks due to

seasonal and diurnal oscillations of Earth's dipole tilt angle (Tsyganenko, 1998). This effect is not captured in our model current sheet, but it is reasonable to expect that if the radius of curvature of the plasma sheet is much larger than the ion inertial scale that it would introduce only small corrections to the present results.

5.2. Reconnection Spreading in Two-Ribbon Solar Flares

Another scenario where the theory may be applicable is in the spreading or “zipper” motion of the ribbons in two-ribbon flares, which is thought to result from out-of-plane spreading of magnetic reconnection in the solar corona (see Qiu et al., 2010, 2017; Tian et al., 2015, and references therein). Qiu et al. (2017) analyzed six two-ribbon flare events that show ribbon elongation/spreading occurs at speeds typically slower than the coronal Alfvén speed by as much as an order of magnitude. One previously known mechanism that could explain a sub-Alfvénic reconnection spreading speed is that the current sheet could have uniform thickness but be thicker than ion inertial scales (Arencibia et al., 2021; Shay et al., 2003). This may be a potential explanation for unidirectional spreading of ribbons with a uniform speed in flare events with a weak guide field, such as fig. 5 in Qiu et al. (2017).

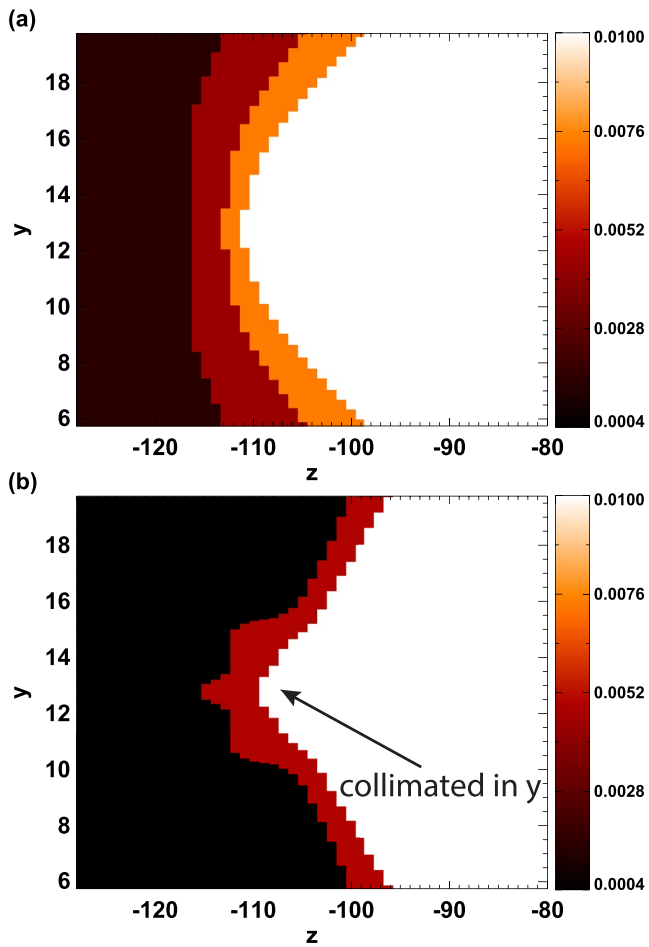


Figure 5. Reconnected magnetic field component B_y in cuts in the yz plane at $x = \bar{x} - L$ for simulations with (a) a current sheet with uniform initial half-thickness of $w_0 = 2$ at $t = 280$ and (b) a current sheet with non-uniform initial thickness with $w_2 = 2$ for $-128 < z < -80$ and $w_1 = 1$ for $-80 < z < 80$ at $t = 170$. B_y is collimated in the y -direction when spreading from a thinner into a thicker current sheet.

The results of the present study provide another mechanism for spreading speeds below the Alfvén speed. An observational signature of this scenario is a reconnection spreading speed that slows with distance. Additionally, if the minimum and maximum half-thicknesses w_1 and w_2 are both larger than the ion inertial scale, the spreading speed is predicted to be both sub-Alfvénic and below the local current carrier speed at any location in the current sheet. This is qualitatively similar to the behavior of observed ribbon elongation speeds in fig. 2 in Qiu et al. (2017) and Fig. 9 in Naus et al. (2022), both showing ribbon elongation speeds varying along the direction of spreading, although we note the former is for an event in which the flare ribbons spread in the direction opposite to that of the inferred current carriers. This signature may potentially be useful for inferring the structure of a reconnecting coronal current sheet as has been alluded to in Naus et al. (2022), even though the thicknesses in question are far below currently resolvable scales in the corona ($d_i \sim 10$ m).

6. Conclusions

We develop a scaling theory of collisionless magnetic reconnection spreading for anti-parallel reconnection with current sheet thicknesses that vary in the out-of-plane direction. Existing theories only apply to current sheets of uniform thickness, predicting that anti-parallel collisionless reconnection spreads at the speed of the local current carriers in the sheet, $v_s = c_A(d_i/w_1)$ for a current sheet of uniform half-thickness w_1 , where c_A is the Alfvén speed based on the reconnecting field and d_i is the ion inertial length. For non-uniform thickness sheets for which reconnection initiates where the half-thickness is w_1 that spreads into a thicker current sheet of half-thickness $w(z)$, we predict that the spreading speed is reduced to $v_s = c_A w_1 d_i / [w(z)]^2$, that is, by a factor of $w_1/w(z)$, due to a reduction in the initial effective reconnecting magnetic field strength (Shay et al., 2004). Therefore, there is a memory effect from the region from which reconnection starts. Importantly, our result provides a mechanism for reconnection spreading slower than the Alfvén and current carrier speeds, which have been inferred from observations in both the solar and magnetospheric settings. For spreading from a thicker to thinner current sheet, the spreading speed is the speed of the current carriers, $v_s = c_A d_i / w(z)$, so there is no memory effect from the region where reconnection begins. We perform a calculation of the timescale of reconnection spreading in a current sheet with a known profile for $w(z)$. We confirm our predictions with 3D two-fluid numerical simulations.

We apply our results to physical systems where the thickness of reconnecting current sheets is known or expected to be initially non-uniform in the out-of-plane direction. In Earth's magnetotail, where the thickness of the near-Earth cross-tail current sheet increases continuously from midnight out to the flank magnetopause, using a model magnetotail shape at active times provides a prediction of the time scale for the spreading. Such an analysis could also be employed for quiet time events, but this was not carried out here. Both predictions should be able to be compared with direct or remote observations, which would be an important step for future work. In two-ribbon solar flares, our result may potentially explain why the ribbons in events with nearly anti-parallel reconnecting fields may spread at sub-Alfvénic speeds. Moreover, we provide an observational signature for spreading in a current sheet with a varying thickness, that is, the speeds change in time during the spreading process. The inferred current sheet thicknesses remain far below current observational capacities, so other approaches will be necessary to confirm or refute the model in solar flares.

There are a number of other avenues for future studies. Our simulations assume the asymptotic reconnecting magnetic field strength is the same everywhere along the current sheet, but this need not be the case. We expect that the results here would carry over with B_0 replaced by $B_x(z)$ in such a scenario, but future work would be

required to test this hypothesis. Simulations in a 3D box geometry may leave out important geometrical effects from realistic systems, including curvature of the magnetic fields and density structure in the solar corona, as well as curvature of the near-Earth magnetotail current sheet during seasonal and diurnal oscillations of the Earth's dipole tilt angle and the normal $B_{z,GSM}$ present in the near-Earth magnetotail. Our study does not include an out-of-plane (guide) magnetic field, which may be relevant in solar flare ribbon spreading events and for the dayside magnetopause and the solar wind. An extension of our results to asymmetric reconnection may also be useful for the study of reconnection spreading at the dayside magnetopause, where it has been reported that the spreading speed of reconnection is sub-Alfvénic (Zou et al., 2018). Generalizing the result to asymmetric reconnection would be necessary to test whether the mechanism discussed here explains the decrease in spreading speed at the dayside magnetopause seen in Walsh et al. (2018), where the current sheet is thinnest near the nose and gets thicker as one goes downtail. The present simulations employ cold electrons within the two-fluid model, so drift waves are absent. In a realistic system, drift waves are expected to potentially be excited where there is a change in the current sheet thickness in the out-of-plane direction. It may be interesting to study reconnection spreading in systems in which the current sheet thickness changes on kinetic scales to see if drift waves play a role and to determine if the equilibrium current prevents spreading. The effect might be expected to be small if the current sheet thickness changes over length scales larger than the electron inertial scale, but studying whether drift waves impact the spreading speed should be the subject of future extended-MHD or kinetic modeling. It would also be interesting to more rigorously describe the effects of embedding in the theory in Section 2.2.

Data Availability Statement

The simulation study was carried out using the two-fluid code F3D (Shay et al., 2004). The model parameters used are detailed in Section 3. Data analysis was carried out, and all simulation figures were generated, with IDL 8.2. Processed simulation data supporting the results and used to generate all simulation figures are publicly available (Arencibia et al., 2022, 2023).

Acknowledgments

The authors acknowledge helpful conversations with Dana Longcope, Toshi Nishimura, Eric Priest, Kathy Reeves, and Luke Shepherd. The authors thank Mahmud Hasan Barbhuiya for assistance with annotating Figure 5. Support from NSF Grants AGS-1460037 (PAC), AGS 1602769 (PAC), AST-1839084 (JQ), AGS-2024198 (MAS), OIA-1655280 (HL), DOE Grant DE-SC0020294 (PAC), NASA Grants 80NSSC19M0146 (PAC), NNX16AG76G (PAC), 80NSSC18K1379 (SMP), 80NSSC20K1813 (MAS), SUB000313/80GSFC19C0027 (HL), SV4-84017 (HL), and 80NSSC21K0003 (HL), and contract 499935Q (SMP) is gratefully acknowledged. Computational resources supporting this work were provided by the NASA High-End Computing (HEC) Program through the NASA Advanced Supercomputing (NAS) Division at Ames Research Center and by the National Energy Research Scientific Computing Center (NERSC), a DOE Office of Science User Facility supported by the Office of Science of the U.S. Department of Energy under Contract no. DE-AC02-05CH11231.

References

- Arencibia, M., Cassak, P. A., Shay, M. A., Qiu, J., Petrinec, S. M., & Liang, H. (2022). Data for three-dimensional reconnection spreading in current sheets of non-uniform thickness [Dataset]. Zenodo. <https://doi.org/10.5281/zenodo.6914761>
- Arencibia, M., Cassak, P. A., Shay, M. A., Qiu, J., Petrinec, S. M., & Liang, H. (2023). Addendum data for three-dimensional reconnection spreading in current sheets of non-uniform thickness [dataset]. Zenodo. <https://doi.org/10.5281/zenodo.7401480>
- Arencibia, M., Cassak, P. A., Shay, M. A., & Priest, E. R. (2021). Scaling theory of three-dimensional magnetic reconnection spreading. *Physics of Plasmas*, 28(8), 082104. <https://doi.org/10.1063/5.0052189>
- Baumjohann, W., Paschmann, G., & Luhr, H. (1990). Characteristics of high-speed ion flows in the plasma sheet. *Journal of Geophysical Research: Space Physics*, 95(A4), 3801–3809. <https://doi.org/10.1029/JA095iA04p03801>
- Cassak, P. A., & Drake, J. F. (2009). The impact of microscopic magnetic reconnection on pre-flare energy storage. *The Astrophysical Journal Letters*, 707(2), L158–L162. <https://doi.org/10.1088/0004-637x/707/2/l158>
- Dorfman, S., Ji, H., Yamada, M., Yoo, J., Lawrence, E., Myers, C., & Tharp, T. D. (2013). Three-dimensional, impulsive magnetic reconnection in a laboratory plasma. *Geophysical Research Letters*, 40(2), 1–238. <https://doi.org/10.1029/2012gl054574>
- Dungey, J. W. (1953). Conditions for the occurrence of electrical discharges in astrophysical systems. *Philosophical Magazine*, 44(354), 725–738. <https://doi.org/10.1080/14786440708521050>
- Egedal, J., Katz, N., Bonde, J., Fox, W., Le, A., Porkolab, M., & Vrublevskis, A. (2011). Spontaneous onset of magnetic reconnection in toroidal plasma caused by breaking of 2D symmetry. *Physics of Plasmas*, 18(11), 111203. <https://doi.org/10.1063/1.3626837>
- Fairfield, D. H. (1979). On the average configuration of the geomagnetic tail. *Journal of Geophysical Research: Space Physics*, 84(A5), 1950–1958. <https://doi.org/10.1029/JA084iA05p01950>
- Fairfield, D. H. (1980). A statistical determination of the shape and position of the geomagnetic neutral sheet. *Journal of Geophysical Research*, 85(A2), 775–780. <https://doi.org/10.1029/ja085ia02p00775>
- Gosling, J. T., Eriksson, S., Blush, L. M., Phan, T. D., Luhmann, J. G., McComas, D. J., et al. (2007). Five spacecraft observations of oppositely directed exhaust jets from a magnetic reconnection X-line extending $> 4.26 \times 10^6$ km in the solar wind at 1 AU. *Geophysical Research Letters*, 34(20), L20108. <https://doi.org/10.1029/2007gl031492>
- Graham, D. R., & Cauzzi, G. (2015). Temporal evolution of multiple evaporating ribbon sources in a solar flare. *The Astrophysical Journal Letters*, 807(2), L22. <https://doi.org/10.1088/2041-8205/807/2/L22>
- Guzdar, P. N., Drake, J. F., McCarthy, D., Hassam, A. B., & Liu, C. S. (1993). Three-dimensional fluid simulations of the nonlinear drift-resistive ballooning modes in tokamak edge plasmas. *Physics of Fluids B*, 5(10), 3712–3727. <https://doi.org/10.1063/1.860842>
- Haaland, S., Reistad, J., Tenfjord, P., Gjerloev, J., Maes, L., DeKeyser, J., et al. (2014). Characteristics of the flank magnetopause: Cluster observations. *Journal of Geophysical Research: Space Physics*, 119(11), 9019–9037. <https://doi.org/10.1002/2014JA020539>
- Hietala, H., Eastwood, J. P., & Isavnin, A. (2014). Sequentially released tilted flux ropes in the earth's magnetotail. *Plasma Physics and Controlled Fusion*, 56(6), 064011. <https://doi.org/10.1088/0741-3335/56/6/064011>
- Hietala, H., Phan, T. D., Angelopoulos, V., Oieroset, M., Archer, M. O., Karlsson, T., & Plaschke, F. (2018). In situ observations of a magnetosheath high-speed jet triggering magnetopause reconnection. *Geophysical Research Letters*, 45(4), 1732–1740. <https://doi.org/10.1002/2017gl076525>
- Huang, K., Liu, Y.-H., Lu, Q., & Hesse, M. (2020). Scaling of magnetic reconnection with a limited x-line extent. *Geophysical Research Letters*, 47(19), e2020GL088147. <https://doi.org/10.1029/2020GL088147>

- Huba, J. D., & Rudakov, L. I. (2002). Three-dimensional Hall magnetic reconnection. *Physics of Plasmas*, 9(11), 4435–4438. <https://doi.org/10.1063/1.1514970>
- Huba, J. D., & Rudakov, L. I. (2003). Hall magnetohydrodynamics of neutral layers. *Physics of Plasmas*, 10(8), 3139–3150. <https://doi.org/10.1063/1.1582474>
- Isobe, H., Yokoyama, T., Shimojo, M., Morimoto, T., Kozu, H., Eto, S., et al. (2002). Reconnection rate in the decay phase of a long duration event flare on 1997 May 12. *The Astrophysical Journal*, 566(1), 528–538. <https://doi.org/10.1086/324777>
- Jain, N., & Büchner, J. (2017). Spreading of electron scale magnetic reconnection with a wave number dependent speed due to the propagation of dispersive waves. *Physics of Plasmas*, 24(8), 082304. <https://doi.org/10.1063/1.4994704>
- Jain, N., Büchner, J., Comişel, H., & Motschmann, U. (2021). Free energy sources in current sheets formed in collisionless plasma turbulence. *The Astrophysical Journal*, 919(2), 103. <https://doi.org/10.3847/1538-4357/ac106c>
- Jain, N., Büchner, J., Dorfman, S., Ji, H., & Sharma, A. S. (2013). Current disruption and its spreading in collisionless magnetic reconnection. *Physics of Plasmas*, 20(11), 112101. <https://doi.org/10.1063/1.4827828>
- Karimabadi, H., Krauss-Varban, D., Huba, J. D., & Vu, H. X. (2004). On magnetic reconnection regimes and associated three-dimensional asymmetries: Hybrid, Hall-less hybrid, and Hall-MHD simulations. *Journal of Geophysical Research*, 109(A9), A09205. <https://doi.org/10.1029/2004ja010478>
- Katz, N., Egedal, J., Fox, W., Le, A., Bonde, J., & Vrublevskis, A. (2010). Laboratory observation of localized onset of magnetic reconnection. *Physical Review Letters*, 104(25), 255004. <https://doi.org/10.1103/physrevlett.104.255004>
- Kaymaz, Z., Siscoe, G., Tsyganenko, N., & Lepping, R. (1994). Magnetotail views at 33 r_e: Imp 8 magnetometer observations. *Journal of Geophysical Research*, 99(A5), 8705–8730. <https://doi.org/10.1029/93JA03564>
- Lapenta, G., Krauss-Varban, D., Karimabadi, H., Huba, J. D., Rudakov, L. I., & Ricci, P. (2006). Kinetic simulations of x-line expansion in 3D reconnection. *Geophysical Research Letters*, 33(10), L10102. <https://doi.org/10.1029/2005gl025124>
- Li, T., Liu, Y.-H., Hesse, M., & Zou, Y. (2020). Three-dimensional x-line spreading in asymmetric magnetic reconnection. *Journal of Geophysical Research: Space Physics*, 125(2), e2019JA027094. <https://doi.org/10.1029/2019JA027094>
- Liu, Y.-H., Li, T. C., Hesse, M., Sun, W., Liu, J., Burch, J., et al. (2019). Three-dimensional magnetic reconnection with a spatially confined X-line extent: Implications for dipolarizing flux bundles and the dawn-dusk asymmetry. *Journal of Geophysical Research: Space Physics*, 124, 2819–2830. <https://doi.org/10.1029/2019JA026539>
- McPherron, R. L., Russell, C. T., & Aubry, M. P. (1973). Phenomenological model for substorms. *Journal of Geophysical Research*, 78(16), 3131–3149. <https://doi.org/10.1029/ja078i016p03131>
- Meyer, J. C., III. (2013). *Structure of the diffusion region in three dimensional magnetic reconnection (Unpublished doctoral dissertation)*. University of Delaware.
- Miyashita, Y., Seki, K., Sakaguchi, K., Hiraki, Y., Nosé, M., Machida, S., et al. (2020). On the transition between the inner and outer plasma sheet in the earth's magnetotail. *Journal of Geophysical Research: Space Physics*, 125(4), e2019JA027561. <https://doi.org/10.1029/2019JA027561>
- Nagai, T. (1982). Observed magnetic substorm signatures at synchronous altitude. *Journal of Geophysical Research*, 87(A6), 4405. <https://doi.org/10.1029/ja087ia06p04405>
- Nagai, T., Shinohara, I., Fujimoto, M., Matsuoka, A., Saito, Y., & Mukai, T. (2011). Construction of magnetic reconnection in the near-earth magnetotail with geotail. *Journal of Geophysical Research: Space Physics*, 116(A4), A04222. <https://doi.org/10.1029/2010JA016283>
- Nagai, T., Shinohara, I., Zenitani, S., Nakamura, R., Nakamura, T. K. M., Fujimoto, M., et al. (2013). Three-dimensional structure of magnetic reconnection in the magnetotail from geotail observations. *Journal of Geophysical Research: Space Physics*, 118(4), 1667–1678. <https://doi.org/10.1002/jgra.50247>
- Nakamura, R., Baumjohann, W., Mouikis, C., Kistler, L., Runov, A., Volwerk, M., et al. (2004). Spatial scale of high-speed flows in the plasma sheet observed by cluster. *Geophysical Research Letters*, 31(9), L09804. <https://doi.org/10.1029/2004gl019558>
- Nakamura, T. K. M., Nakamura, R., Alexandrova, A., Kubota, Y., & Nagai, T. (2012). Hall magnetohydrodynamic effects for three-dimensional magnetic reconnection with finite width along the direction of the current. *Journal of Geophysical Research*, 117(A3), 03220. <https://doi.org/10.1029/2011ja017006>
- Naus, S. J., Qiu, J., DeVore, C. R., Antiochos, S. K., Dahlin, J. T., Drake, J. F., & Swisdak, M. (2022). Correlated spatio-temporal evolution of extreme-ultraviolet ribbons and hard X-rays in a solar flare. *The Astrophysical Journal*, 926(2), 218. <https://doi.org/10.3847/1538-4357/ac4028>
- Ng, J., Chen, L.-J., & Omelchenko, Y. A. (2021). Bursty magnetic reconnection at the earth's magnetopause triggered by high-speed jets. *Physics of Plasmas*, 28(9), 092902. <https://doi.org/10.1063/5.0054394>
- Phan, T. D., Gosling, J. T., Davis, M. S., Skoug, R. M., Oieroset, M., Lin, R. P., et al. (2006). A magnetic reconnection X-line extending more than 390 Earth radii in the solar wind. *Nature*, 439(7073), 175–178. <https://doi.org/10.1038/nature04393>
- Priest, E., & Forbes, T. (2000). *Magnetic reconnection*. Cambridge University Press.
- Qiu, J. (2009). Observational analysis of magnetic reconnection sequence. *The Astrophysical Journal*, 692(2), 1110–1124. <https://doi.org/10.1088/0004-637x/692/2/1110>
- Qiu, J., Liu, W., Hill, N., & Kazachenko, M. (2010). Reconnection and energetics in two-ribbon flares: A revisit of the Bastille Day flare. *The Astrophysical Journal*, 725(1), 319–330. <https://doi.org/10.1088/0004-637x/725/1/319>
- Qiu, J., Longcope, D. W., Cassak, P. A., & Priest, E. R. (2017). Elongation of flare ribbons. *The Astrophysical Journal*, 838(1), 17. <https://doi.org/10.3847/1538-4357/aa6341>
- Rogers, A. J., Farrugia, C. J., Torbert, R. B., & Rogers, T. J. (2023). Applying magnetic curvature to MMS data to identify thin current sheets relative to tail reconnection. *Journal of Geophysical Research: Space Physics*, 128(1), e2022JA030577. <https://doi.org/10.1029/2022JA030577>
- Rong, Z. J., Wan, W. X., Shen, C., Li, X., Dunlop, M. W., Petrukovich, A. A., et al. (2011). Statistical survey on the magnetic structure in magnetotail current sheets. *Journal of Geophysical Research: Space Physics*, 116(A9), A09218. <https://doi.org/10.1029/2011JA016489>
- Sergeev, V. A., Tanskanen, P., Mursula, K., Korh, A., & Elphic, R. C. (1990). Current sheet thickness in the near-Earth plasma sheet during substorm growth phase. *Journal of Geophysical Research*, 95(A4), 3819–3828. <https://doi.org/10.1029/JA095iA04p03819>
- Shay, M. A., Drake, J. F., Swisdak, M., Dorland, W., & Rogers, B. N. (2003). Inherently three-dimensional magnetic reconnection: A mechanism for bursty bulk flows? *Geophysical Research Letters*, 30(6), 1345. <https://doi.org/10.1029/2002gl016267>
- Shay, M. A., Drake, J. F., Swisdak, M., & Rogers, B. N. (2004). The scaling of embedded collisionless reconnection. *Physics of Plasmas*, 11(5), 2199–2213. <https://doi.org/10.1063/1.1705650>
- Shepherd, L. S., & Cassak, P. A. (2012). Guide field dependence of 3D X-line spreading during collisionless magnetic reconnection. *Journal of Geophysical Research*, 117(A10), A10101. <https://doi.org/10.1029/2012ja017867>
- Shepherd, L. S., Cassak, P. A., Drake, J. F., Gosling, J. T., Phan, T.-D., & Shay, M. A. (2017). Structure of exhausts in magnetic reconnection with an x-line of finite extent. *The Astrophysical Journal*, 848(2), 90. <https://doi.org/10.3847/1538-4357/aa9066>

- Tian, H., Young, P. R., Reeves, K. K., Chen, B., Liu, W., & McKillop, S. (2015). Temporal evolution of chromospheric evaporation: Case studies of the M1.1 Flare on 2014 September 6 and X1.6 Flare on 2014 September 10. *The Astrophysical Journal*, *811*(2), 139. <https://doi.org/10.1088/0004-637X/811/2/139>
- Tripathi, D., Isobe, H., & Mason, H. E. (2006). On the propagation of brightening after filament/prominence eruptions, as seen by SoHO-EIT. *Astronomy & Astrophysics*, *453*(3), 1111–1116. <https://doi.org/10.1051/0004-6361:20064993>
- Tsyganenko, N. A. (1998). Modeling of twisted/warped magnetospheric configurations using the general deformation method. *Journal of Geophysical Research*, *103*(A10), 23551–23564. <https://doi.org/10.1029/98JA02292>
- Vasyliunas, V. M. (1975). Theoretical models of magnetic field line merging, 1. *Reviews of Geophysics*, *13*(1), 303. <https://doi.org/10.1029/rg013i001p00303>
- Voigt, G. H. (1984). The shape and position of the plasma sheet in earth's magnetotail. *Journal of Geophysical Research*, *89*(A4), 2169–2179. <https://doi.org/10.1029/JA089iA04p02169>
- Walsh, B. M., Welling, D. T., Zou, Y., & Nishimura, Y. (2018). A maximum spreading speed for magnetopause reconnection. *Geophysical Research Letters*, *45*(11), 5268–5273. <https://doi.org/10.1029/2018GL078230>
- Zhou, M., Ashour-Abdalla, M., Deng, X., Pang, Y., Fu, H., Walker, R., et al. (2017). Observation of three-dimensional magnetic reconnection in the terrestrial magnetotail. *Journal of Geophysical Research: Space Physics*, *122*(9), 9513–9520. <https://doi.org/10.1002/2017JA024597>
- Zou, Y., Walsh, B. M., Nishimura, Y., Angelopoulos, V., Ruohoniemi, J. M., McWilliams, K. A., & Nishitani, N. (2018). Spreading speed of magnetopause reconnection x-lines using ground-satellite coordination. *Geophysical Research Letters*, *45*(1), 80–89. <https://doi.org/10.1002/2017GL075765>

Erratum

Since the original publication of this article, references for Isobe et al. (2002), Liu et al. (2019), Qiu et al. (2009), Qiu et al. (2010), and Shepherd et al. (2017) have been updated for the correct citation information. Also, the image for Figure 4 has been updated to remove the crossout of the legend box in the top right. This may be considered the authoritative version of record.